

Non-Newtonian, non-isothermal three-dimensional modeling of strand deposition in screw-based material extrusion

Alessio Pricci^{1,2 a *}, Gianluca Percoco^{2,3 b}

¹ Department of Electrical and Information Engineering (DEI), Polytechnic University of Bari, Via E. Orabona 4, 70125 Bari, Italy

² Interdisciplinary Additive Manufacturing (IAM) Lab, Polytechnic University of Bari, Viale del Turismo 8, 74100 Taranto, Italy

³ Department of Mechanics, Mathematics and Management (DMMM), Polytechnic University of Bari, Via E. Orabona 4, 70125 Bari, Italy

^aalessio.pricci@poliba.it, ^bgianluca.percoco@poliba.it

Keywords: Additive Manufacturing, Pellet Extrusion, Virtual Modeling

Abstract. Material extrusion (MEX) is one of the most widespread additive manufacturing techniques. Among the MEX processes, pellet additive manufacturing (PAM) is of primary interest in industry 4.0 scenario, mainly because of the lower unit cost, energy consumption and waste production, together with the wider range of printable materials. Mechanical properties are related to the intra and inter layer bonding, which in turn depends on the strand geometry. For the first time, the relationship between PAM processing parameters and layer morphology has been studied by means of non-Newtonian, non-isothermal three-dimensional numerical simulations; the influence on mass flow rate and strand shape has been investigated. A very good correspondence between experiments and numerical computations of layer shape was found. Thermal contact area increases at lower layer heights, but counterpressure limits the extruded mass flow rate. This effect can be mitigated by choosing higher barrel temperatures and screw speed.

Introduction

In internet of things era, the production has become much more flexible, efficient and automated than in the past. In the framework of the upcoming industry 4.0 revolution (4IR), additive manufacturing (AM) represents one of the key pillars [1–3].

The most beneficial aspects of AM for 4IR are the reduction of wastes, energy requested [4] and prototyping times [5], together with an increase in product customization, the change of supply chain and its management [6], and the possibility to digitalize the manufacturing activity, creating a digital twin of the process [7].

Among material extrusion (MEX) techniques, both fused filament fabrication (FFF) and pellet additive manufacturing (PAM) are of primary interest. The first consists in the gradual melting of thermoplastic material, given in the form of a solid filament, and its deposition on a build plate. Instead, in PAM a screw extruder melts and convey a pelletized feedstock [8]. Some of the main applications are in automotive [9], tooling [10], renewable energies [11], and buildings [12].

In recent years, computational fluid dynamics (CFD) has been established as a very promising way to gain a better insight of MEX processes [13–28].

The first studies were dedicated to FFF; the main works are briefly described, because they are the basis for PAM modeling. In [13] the strand morphology has been analysed at varying layer height and printing speed; this work was experimentally validated in [14]. The numerical investigation was extended in [15,16] to study the corner MEX according to different strategies. Moreover, in [17,18] the interlayer contact between deposited strand has been analysed, yet disregarding the filament coalescence; in addition, the influence of temperature has been

neglected. A different approach for single strand deposition was proposed in [19], where an improvement of the results of [13] is found by considering energy equation. The successive layer deposition has been simulated in [20,21], to predict the cooling time and inter-layer contact area. In [22] both single and multi-layer deposition in FFF, together with a study of the solidification process, are presented under the assumption of considering a Newtonian fluid.

More recently, CFD has proved as a powerful tool to study PAM process. Some of the main perspectives are the prediction of final part properties, manufactured both with net and composite materials, and the individuation of the optimal process parameters [23].

In [24] the strand deposition for different rheological models was simulated: the most important aspect which affects strand morphology in PAM is the inclusion of the shear-thinning behaviour in simulations. In [25] the effect of successive layer deposition has been studied with a remeshing technique performed via the Comsol-MATLAB LiveLink [26]. Despite the authors propose a two-dimensional simulation, it gives important insights in layer coalescence, through non-isothermal simulations. Moreover, a good agreement with optical micrographs is shown. Thermodynamic aspects related to reheating of the deposited strand caused by the heated nozzle have been addressed in [27]; here, heat transfer has been coupled with fluid flow equations and studied numerically. Infrared thermography provided a very good correspondence with FEM predictions. Up to now, the three-dimensional investigation of the strand deposition has not been done, when dealing with PAM, even if one considers the deposition of net polymers.

In this work the strand deposition in PAM extrusion has been investigated with both experiments and CFD simulations. A Direct 3D pellet extruder has been used to print consistent layers under different values of the most critical printing parameters, that are the dimensionless printing speed (V^*), layer height (D^*), and nozzle temperature (T^*).

CFD analyses have been performed by means of non-Newtonian, non-isothermal three-dimensional simulations; the main aim was to model the effect of the abovementioned processing parameters on strand morphologies.

At first, the material properties were introduced in section “Material”. The experimental setup has been detailed in section “Experimental validation”, where the values assigned to the process parameters have been stated. In section “Numerical investigations” full details about the multiphase simulations are given. The effect of process parameters on extruded mass flow rate is investigated in section “Mass flow rate”; then, the effect of dimensionless parameters on strand cross-section has been explored in section “Strand morphology”. Finally, conclusions and further works have been outlined.

Materials and methods

In this section, the relevant material’s properties have been introduced. Then, full details on experimental and CFD investigations have been given.

Material.

In this study, a particular grade of polylactic acid (PLA) manufactured by NatureWorks (NatureWorks Ingeo 3251D) has been used to investigate the first layer deposition on a heated build plate in PAM extrusion. The material is initially given in the form of almost spherical pellet of around 3 [mm] diameter.

The parameters involved in CFD simulations are:

- Rheological properties
 - Dynamic viscosity, which is a function of both temperature and shear rate, $\eta(T; \dot{\gamma})$, and
 - Glass transition temperature, T_g .

- Thermophysical properties
 - Density at solid (ρ_s) and molten (ρ_m) states,
 - thermal conductivity, $\lambda(T)$, and
 - heat capacity $c_p(T)$,

Temperature-dependent behavior of abovementioned properties was modeled with Moldflow software (Moldflow Plastics Labs. Ithaca, NY 14850, USA).

Experimental investigation.

A Direct 3D PAM extruder (Direct 3D s.r.l.) has been employed to study the first layer deposition under a wide set of process parameters.

The extruder consists of a constant pitch screw placed inside a heated barrel. At first, the pelletized material is conveyed in a hopper. Then, it is gradually heated above T_g . Finally, the molten polymer is extruded through a nozzle, to be deposited layer-by-layer, as in FFF.

The mechanical torque is provided by a Nema17 HS4401 stepper motor, to be delivered to the vertical screw by means of a timing belt.

The pressure starts to rise in the solid-conveying zone, up to the last screw vanes. Then, it drops in the nozzle and deposited layer, up to the atmospheric value [29].

The most important extrusion parameters in MEX layer deposition are nozzle outlet diameter (D), layer height (h), printing speed (V_p), flow rate (fr%) and both nozzle (T_n) and build plate (T_b) temperatures.

To be said, for a given flow rate, the screw peripheral speed (V_s) is set; for that reason, it will be referred directly to this parameter.

On this basis, the minimal set of dimensionless parameters are:

- $H^* = h/D$,
- $T^* = T_n/T_b$, and
- $V^* = V_s/V_p$

In all investigations, V_p and T_b were fixed to 20 [mm/s] and 60 [°C], respectively. Moreover, $D = 1.2$ [mm].

Two nozzle temperatures (190 and 210 [°C]), two flow rate values (500 and 1000 %, that result in 30 and 60 [rpm], respectively) and three layer heights (0.3, 0.6 and 0.9 [mm]) have been examined.

A total of 12 investigations were carried out (Table 1):

Table 1. Full set of experimental dimensionless printing conditions

| Index | T* | D* | V* | Index | T* | D* | V* |
|--------------|-----------|-----------|-----------|--------------|-----------|-----------|-----------|
| 1 | 3.15 | 0.25 | 0.95 | 7 | 3.5 | 0.25 | 0.95 |
| 2 | 3.15 | 0.25 | 1.89 | 8 | 3.5 | 0.25 | 1.89 |
| 3 | 3.15 | 0.5 | 0.95 | 9 | 3.5 | 0.5 | 0.95 |
| 4 | 3.15 | 0.5 | 1.89 | 10 | 3.5 | 0.5 | 1.89 |
| 5 | 3.15 | 0.75 | 0.95 | 11 | 3.5 | 0.75 | 0.95 |
| 6 | 3.15 | 0.75 | 1.89 | 12 | 3.5 | 0.75 | 1.89 |

The experimental workflow for a generic printing condition has been reported in Fig.1:

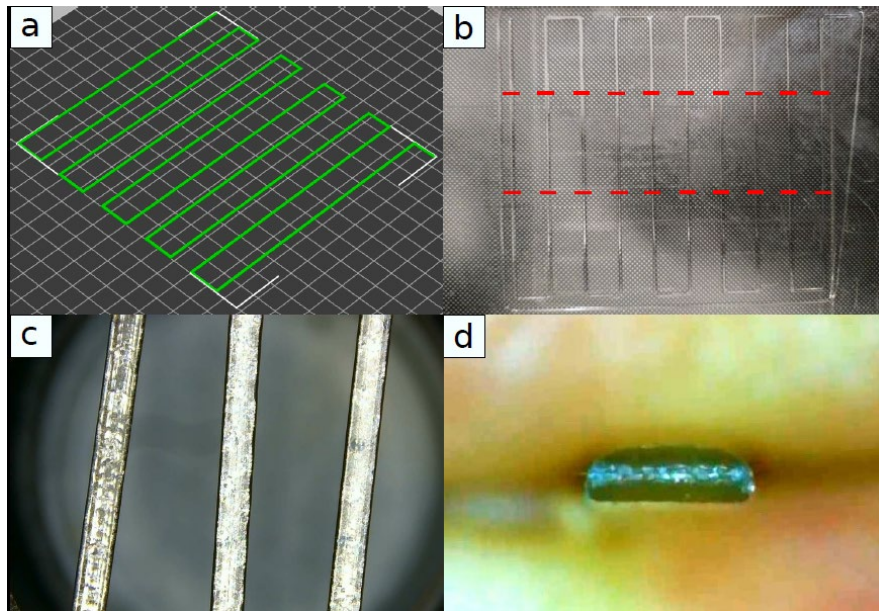


Fig. 1. a.) Serpentine geometry; b.) Printed samples with indication of trim start and stop; c) trimmed samples at microscope; d.) Best sample cross-section

At first, a serpentine geometry was printed (Fig.1a): a total of 10 straight layers were cut (Fig.1b) and their widths were analyzed to provide replications (Fig.1c); a Tomlov DM11 7'' optical microscope was used for investigating strands' geometries.

For a given printing condition, the mean and standard deviation of strand width were estimated, together with the coefficient of variation (COV): a low COV (<10) was found in all printing conditions, which confirmed the consistency of first strand deposition.

Then, the relative deviation of each strand width from mean value was calculated, to find the best one; its cross-section (Fig.1d) was observed through the microscope.

The cross-sectional area (A_s) was calculated with a MATLAB subroutine and the mean velocity in the nozzle calibration zone was evaluated by mass flow rate conservation from nozzle outlet to the deposited strand:

$$u_m = 4 \frac{A_s}{\pi D^2} V_p \frac{\rho_s}{\rho_m} \quad (1)$$

In previous equation, ρ_s and ρ_m are solid and molten polymer densities, respectively. The mean velocity values were the input boundary conditions for CFD studies.

Numerical investigations.

The CFD analyses were performed with the commercial finite volume method (FVM) software Ansys Fluent.

The computational domain consists of the nozzle calibration zone, the air gap between the nozzle outlet and build plate. The nozzle tip geometry was taken out from the original rectangular domain (Fig.2).

The screw tip was not included in the computational domain because swirling motion does not influence the flow field, at least for net polymers [30].

A structured mesh with hexahedral elements was adopted; their number was gradually inflated near the nozzle outlet and build plate, to fully capture the local boundary layer regions.

For instance, the CFD modeling of the $D^* = 0.25$ case has been reported in Fig.2:

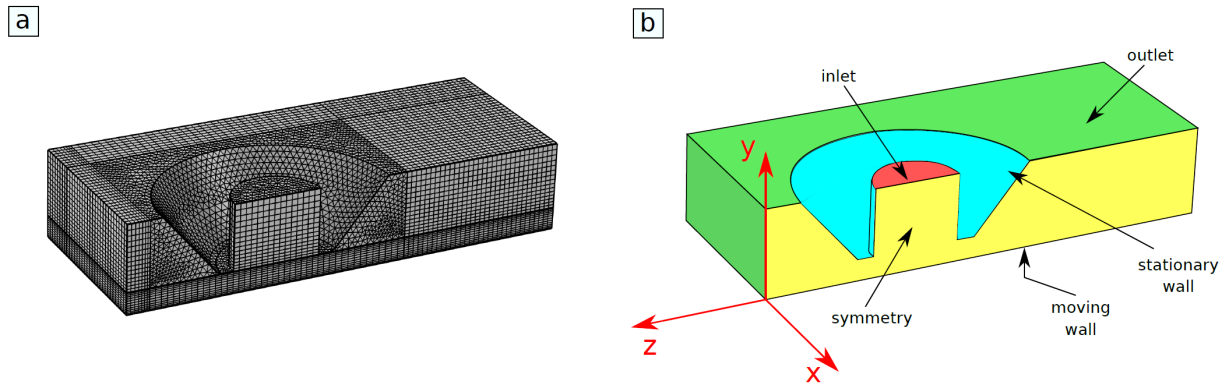


Fig. 2. a.) Meshed domain and b.) boundary conditions and reference system

For CFD simulations, only half of the geometry was considered due to the domain symmetry. The modeling of flow deposition is three-dimensional, non-isothermal and aimed at capturing the non-Newtonian flow behavior. In fact, it has been shown [24] that the most important factor which affects the strand shape is the inclusion of the non-Newtonian behavior, instead of the actual rheological model.

The boundary conditions have been highlighted in Fig.2b. The printing speed is assigned to the build plate instead of the nozzle, to avoid domain remeshing.

An implicit numerical scheme with interfacial anti-diffusion and implicit body force was adopted; the interface between the molten polymer and surrounding air was captured by means of the volume of fluid (VOF) method, because of its robustness in free-surface tracking.

A second order upwind scheme was adopted to discretize momentum and energy equations, to lower numerical diffusion, while the compressive method was used for the continuity equation of the volume fraction of the VOF method.

Only the volume fraction threshold residual was lowered to $1e-6$ (default value was $1e-5$), to achieve a better approximation of the interface.

The time-stepping was automatically set to guarantee a Courant number of 0.25, so to enhance numerical stability. The overall study stops after finding the steady state extrudate profile.

Results and discussion

In this section, the comparison between experiments and CFD in all extrusion conditions has been made.

Fluent has been widely used for this purpose, when dealing with sub millimetric nozzle diameters and conventional FFF [13,14].

In other works, a 2D approach has been detailed [30–33], to deal with screw-based thermoplastic MEX. In [24] a 3D model has been proposed, but the study does not account for the effect of temperature, and it is limited to a single printing condition.

Instead, the interaction of the minimum set of dimensionless parameters is here considered (Table 1): a full-factorial experimental and numerical design of experiment has been adopted for this purpose.

Mass flow rate.

Before proceeding with the investigation of CFD results, the effect of nozzle temperature, layer height and screw speed on mass flow rate has been investigated (Fig.3).

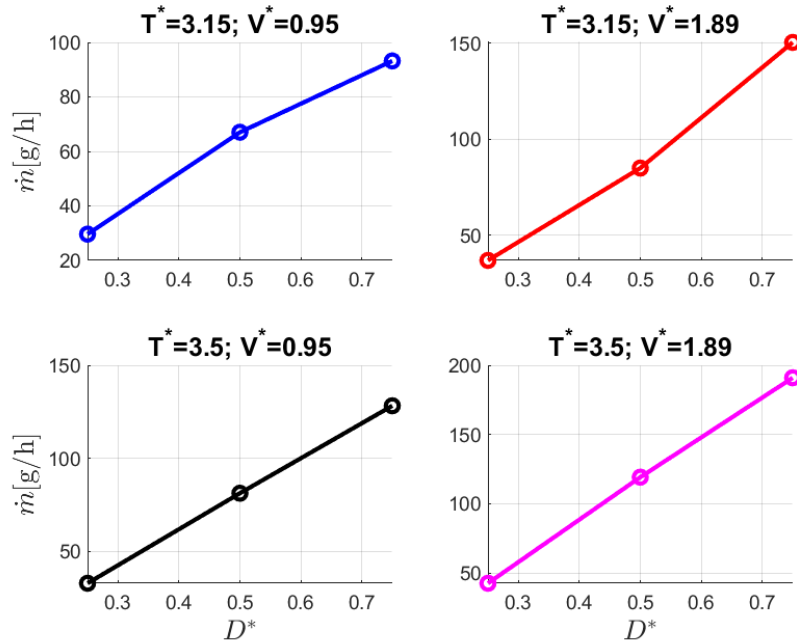


Fig. 3. Mean extruded mass flow rate at different values of the operating parameters; \dot{m} : mass flow rate

At increasing D^* , mass flow rate rises almost linearly; this is due to the lower counterpressure which develops in PAM extrusion [29].

The same trend applies for T^* , but it is due to the lower viscosity in the nozzle calibration zone. In addition, mass flow rate increases with V^* , no matter of the nozzle temperature and layer height.

Strand morphology.

The analysis starts with the mean inlet speed evaluation (see: Eq. 1), calculated through the experimental measurement of cross-sectional areas. Then, the mean flow velocity in the nozzle calibration zone was used as inlet condition (Fig.2b) in CFD computations.

A difference with conventional FFF is that the layer width set in the slicing software is different from that found experimentally, as will be seen in next figure; this is caused by the operating mechanism of the Direct 3D PAM extruder, where the flow rate percentage directly controls the screw rotation, and so the mass flow rate.

Instead, in FFF the mass flow rate calculation is straightforward; for prescribed layer height and width, mass flow rate can be evaluated by one-dimensional continuity principle.

In Fig.4 the comparison between numerical and experimental cross-sectional profiles has been done; X^* and Y^* are the absolute reference system coordinates (Fig.2), made dimensionless with respect to the nozzle outer diameter.

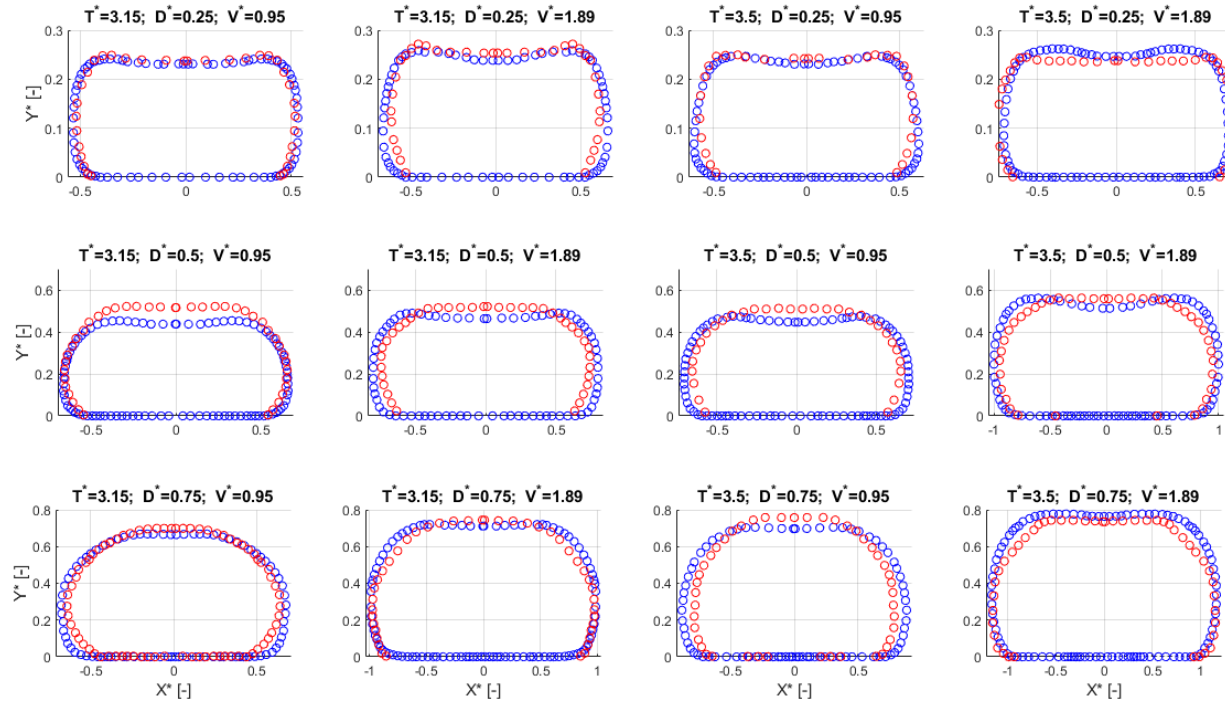


Fig. 4. Experimental (red) and numerical (blue) cross-section profiles of the deposited strands at different processing conditions (see Table 1)

Overall strand shape is fully captured by the chosen numerical setup. The maximum strand width in CFD is slightly lower than in experiments, especially at $D^* = 0.5$. A possible reason can be related to having disregarded the actual viscoelastic behavior.

By lowering D^* , a more oblong cross-sectional shape is found [13], which determines a broader interface for thermal diffusion, which is necessary to create strong inter-layer bonds.

On the other hand, the circular-like shape which arises at high D^* is well captured by FVM.

Moreover, T^* impact deeply layer shape [19]; an increase of this parameter leads to broader layer widths, together with a central collapse of the upper part of the layer, probably caused by the Newtonian-like behavior of PLA at high temperatures.

The effect of V^* on cross-section shape is the most noticeable; an increase in V^* means a higher mass flow rate and strand width increases consequently; a quantitative analysis based on CFD computations has been reported in Table 2:

Table 2. Increase in maximum layer width (W_{max}) when switching from low to high V^*

| D^* | T^* | Low V^* | W_{max} at low V^* [μm] | High V^* | W_{max} at high V^* [μm] | Increase in W_{max} switching from low to high V^* [%] |
|-------|-------|-----------|---|---------------|--|--|
| 0.25 | 3.15 | 0.95 | 1290 | 1.89 | 1552 | 20.31 |
| 0.25 | 3.5 | 0.95 | 1460 | 1.89 | 1702 | 16.57 |
| 0.5 | 3.15 | 0.95 | 1572 | 1.89 | 1933 | 22.96 |
| 0.5 | 3.5 | 0.95 | 1754 | 1.89 | 2400 | 36.83 |
| 0.75 | 3.15 | 0.95 | 1612 | 1.89 | 2237 | 38.77 |
| 0.75 | 3.5 | 0.95 | 2100 | 1.89 | 2820 | 34.28 |

The maximum layer width increases with layer height and temperature. The first trend is related to the lower counterpressure (and consequently, higher mass flow rate, see Fig.3) which develops at high layer heights [29]. The second one is motivated by the more Newtonian-like behavior of the deposited material; it undergoes a larger radial squeezing at higher nozzle temperatures because of the lower viscosity.

Conclusions and further works

A numerical and experimental workflow for PAM extrusion has been presented and validated with respect to different operating conditions.

A systematic method for the evaluation of the cross-section of the first deposited strand has been proposed. The method differs from the ones conventionally proposed for FFF, where the mass flow rate can be calculated by the flow parameter set in the slicing software. In PAM extrusion, the flow parameter is related to the screw peripheral speed, which is the key factor affecting mass flow rate and layer width: the exact layer width imposed in slicing software can't be generally met, because a variation in screw speed results in a different extruded mass flow rate.

The effect of dimensionless layer height (D^*), temperature (T^*) and speed (V^*) on mass flow rate and strand shape was investigated.

The D^* parameter has a deep impact on the mechanical properties of the printed part; in fact, by lowering D^* , higher surface finish can be generally reached; this is caused by the higher thermal contact area provided by the resulting oblong strand shape. However, the mass flow rate conveyed by the screw-barrel system at small D^* is low because of the higher counterpressure. Nevertheless, the reduction in mass flow rate at small D^* can be mitigated by choosing higher barrel temperatures.

On the other hand, higher D^* produce more circular-like shaped strands, with very low thermal contact areas. In addition, higher productivity can be achieved because of a very low counterpressure.

Dimensionless temperature T^* was varied on two levels in the suggested interval for PLA; increasing T^* lead to higher layer width and lower height (top collapse), together with higher mass flow rates. This is probably caused by the Newtonian-like flow behavior, which shows up at higher T^* .

Finally, higher V^* lead to wider radial squeezing, when layer is deposited on the build plate because of the higher mass flow rate which is delivered by the screw-barrel system.

In general, it has been shown a good agreement between numerical and experimental results, proving CFD as a milestone in establishing a digital twin for PAM.

In further work, the investigation will be carried out for fiber-reinforced polymers, which are of remarkable interest for PAM because of the improved parts' mechanical properties, such as the overall strength and surface accuracy, driven by the flow fiber alignment.

References

- [1] U.M. Dilberoglu, B. Gharehpapagh, U. Yaman, M. Dolen, The Role of Additive Manufacturing in the Era of Industry 4.0, *Procedia Manuf.* 11 (2017) 545–554. <https://doi.org/10.1016/j.promfg.2017.07.148>
- [2] A. Haleem, M. Javaid, Additive Manufacturing Applications in Industry 4.0: A Review, *Journal of Industrial Integration and Management.* 04 (2019) 1930001. <https://doi.org/10.1142/S2424862219300011>
- [3] J. Butt, Exploring the Interrelationship between Additive Manufacturing and Industry 4.0, *Designs (Basel).* 4 (2020) 13. <https://doi.org/10.3390/designs4020013>
- [4] Post B. K., Lind R. F., Lloyd P. D., Kunc V., Linhal J. M., Love L. J., The Economics of Big Area Additive Manufacturing, in: *Solid Freeform Fabrication 2016: Proceedings of the 26th Annual International Solid Freeform Fabrication Symposium – An Additive Manufacturing Conference, 2016.*
- [5] S. Chong, G.-T. Pan, J. Chin, P. Show, T. Yang, C.-M. Huang, Integration of 3D Printing and Industry 4.0 into Engineering Teaching, *Sustainability.* 10 (2018) 3960. <https://doi.org/10.3390/su10113960>
- [6] M. Attaran, Additive Manufacturing: The Most Promising Technology to Alter the Supply Chain and Logistics, *Journal of Service Science and Management.* 10 (2017) 189–206. <https://doi.org/10.4236/jssm.2017.103017>
- [7] L. Zhang, X. Chen, W. Zhou, T. Cheng, L. Chen, Z. Guo, B. Han, L. Lu, Digital twins for additive manufacturing: A state-of-the-art review, *Applied Sciences (Switzerland).* 10 (2020) 1–10. <https://doi.org/10.3390/app10238350>
- [8] A. Pricci, M.D. de Tullio, G. Percoco, Analytical and Numerical Models of Thermoplastics: A Review Aimed to Pellet Extrusion-Based Additive Manufacturing, *Polymers, Vol. 13, Page 3160.* 13 (2021) 3160. <https://doi.org/10.3390/POLYM13183160>
- [9] F. Talagani, C. Godines, Numerical Simulation of Big Area Additive Manufacturing (3D Printing) of a Full Size Car, 2015.
- [10] B.K. Post, P.C. Chesser, R.F. Lind, A. Roschli, L.J. Love, K.T. Gaul, M. Sallas, F. Blue, S. Wu, Using Big Area Additive Manufacturing to directly manufacture a boat hull mould, *Virtual Phys Prototyp.* 14 (2019) 123–129. <https://doi.org/10.1080/17452759.2018.1532798>
- [11] B.K. Post, B. Richardson, R. Lind, L.J. Love, P. Lloyd, V. Kunc, B.J. Rhyne, A. Roschli, J. Hannan, S. Nolet, K. Veloso, P. Kurup, T. Remo, D. Jenne, *Big Area Additive Manufacturing Application in Wind Turbine Molds, 2017.*
- [12] J. Pasco, Z. Lei, C. Aranas, Additive Manufacturing in Off-Site Construction: Review and Future Directions, *Buildings.* 12 (2022) 53. <https://doi.org/10.3390/buildings12010053>
- [13] R. Comminal, M.P. Serdeczny, D.B. Pedersen, J. Spangenberg, Numerical modeling of the strand deposition flow in extrusion-based additive manufacturing, *Addit Manuf.* 20 (2018) 68–76. <https://doi.org/10.1016/j.addma.2017.12.013>

- [14] M.P. Serdeczny, R. Comminal, D.B. Pedersen, J. Spangenberg, Experimental validation of a numerical model for the strand shape in material extrusion additive manufacturing, *Addit Manuf.* 24 (2018) 145–153. <https://doi.org/10.1016/j.addma.2018.09.022>
- [15] R. Comminal, M.P. Serdeczny, D.B. Pedersen, J. Spangenberg, Motion planning and numerical simulation of material deposition at corners in extrusion additive manufacturing, *Addit Manuf.* 29 (2019) 100753. <https://doi.org/10.1016/j.addma.2019.06.005>
- [16] R. Comminal, M.P. Serdeczny, D.B. Pedersen, J. Spangenberg, Numerical modeling of the material deposition and contouring in fused deposition modeling, in: *Solid Freeform Fabrication 2018: Proceedings of the 29th Annual International (Ed.)*, Solid Freeform Fabrication 2018: Proceedings of the 29th Annual International, 2018.
- [17] M.P. Serdeczny, R. Comminal, D.B. Pedersen, J. Spangenberg, Numerical simulations of the mesostructure formation in material extrusion additive manufacturing, *Addit Manuf.* 28 (2019) 419–429. <https://doi.org/10.1016/j.addma.2019.05.024>
- [18] R. Comminal, S. Jafarzadeh, M. Serdeczny, J. Spangenberg, Estimations of Interlayer Contacts in Extrusion Additive Manufacturing Using a CFD Model, in: *Industrializing Additive Manufacturing*, Springer International Publishing, Cham, 2021: pp. 241–250. https://doi.org/10.1007/978-3-030-54334-1_17
- [19] B. Behdani, M. Senter, L. Mason, M. Leu, J. Park, Numerical Study on the Temperature-Dependent Viscosity Effect on the Strand Shape in Extrusion-Based Additive Manufacturing, *Journal of Manufacturing and Materials Processing.* 4 (2020) 46. <https://doi.org/10.3390/jmmp4020046>
- [20] J. Du, Z. Wei, X. Wang, J. Wang, Z. Chen, An improved fused deposition modeling process for forming large-size thin-walled parts, *J Mater Process Technol.* 234 (2016) 332–341. <https://doi.org/10.1016/j.jmatprotec.2016.04.005>
- [21] H. Xia, J. Lu, G. Tryggvason, Fully resolved numerical simulations of fused deposition modeling. Part II – solidification, residual stresses and modeling of the nozzle, *Rapid Prototyp J.* 24 (2018) 973–987. <https://doi.org/10.1108/RPJ-11-2017-0233>
- [22] E.P. Furlani, V. Sukhotskiy, A. Verma, V. Vishnoi, P. Amiri Roodan, Numerical Simulation of Extrusion Additive Manufacturing: Fused Deposition Modeling, *TechConnect Briefs.* 4 (2018) 118–121.
- [23] T.G. Crisp, Weaver Jason M., Review of Current Problems and Developments in Large Area Additive Manufacturing (LAAM), in: *Solid Freeform Fabrication 2021: Proceedings of the 32nd Annual International Solid Freeform Fabrication Symposium – An Additive Manufacturing Conference*, 2021.
- [24] R. Comminal, M.P. Serdeczny, N. Ranjbar, M. Mehrali, D.B. Pedersen, H. Stang, J. Spangenberg, Modelling of material deposition in big area additive manufacturing and 3D concrete printing, in: *Joint Special Interest Group Meeting between Euspen and ASPE*, 2019. www.euspen.eu
- [25] A.-D. Le, B. Cosson, A.C.A. Asséko, Simulation of large-scale additive manufacturing process with a single-phase level set method: a process parameters study, *The International Journal of Advanced Manufacturing Technology.* 113 (2021) 3343–3360. <https://doi.org/10.1007/s00170-021-06703-5>
- [26] Comsol Multiphysics, LiveLink™ for MATLAB® User's Guide, 2009. www.comsol.com/blogs

- [27] B. Cosson, A.C. Akué Asséko, L. Pelzer, C. Hopmann, Radiative Thermal Effects in Large Scale Additive Manufacturing of Polymers: Numerical and Experimental Investigations, *Materials*. 15 (2022) 1052. <https://doi.org/10.3390/ma15031052>
- [28] A. Pricci, M.D. de Tullio, G. Percoco, Semi-analytical models for non-Newtonian fluids in tapered and cylindrical ducts, applied to the extrusion-based additive manufacturing, *Mater Des*. 223 (2022) 111168. <https://doi.org/10.1016/j.matdes.2022.111168>
- [29] A. Pricci, M.D. de Tullio, G. Percoco, Modeling of extrusion-based additive manufacturing for pelletized thermoplastics: Analytical relationships between process parameters and extrusion outcomes, *CIRP J Manuf Sci Technol*. 41 (2023) 239–258. <https://doi.org/10.1016/j.cirpj.2022.11.020>
- [30] Z. Wang, D.E. Smith, Numerical analysis of screw swirling effects on fiber orientation in large area additive manufacturing polymer composite deposition, *Compos B Eng*. 177 (2019) 107284. <https://doi.org/10.1016/J.COMPOSITESB.2019.107284>
- [31] Z. Wang, D.E. Smith, Rheology Effects on Predicted Fiber Orientation and Elastic Properties in Large Scale Polymer Composite Additive Manufacturing, *Journal of Composites Science*. 2 (2018) 10. <https://doi.org/10.3390/jcs2010010>
- [32] Z. Wang, D.E. Smith, A Fully Coupled Simulation of Planar Deposition Flow and Fiber Orientation in Polymer Composites Additive Manufacturing, *Materials*. 14 (2021) 2596. <https://doi.org/10.3390/ma14102596>
- [33] Z. Wang, D.E. Smith, Finite element modelling of fully-coupled flow/fiber-orientation effects in polymer composite deposition additive manufacturing nozzle-extrudate flow, *Compos B Eng*. 219 (2021) 108811. <https://doi.org/10.1016/j.compositesb.2021.108811>